

## Article

# First Approach to Doping Silver into CrB<sub>2</sub> Thin Films Deposited by DC/HiPIMS Technology in Terms of Mechanical and Tribological Properties

Martin Truchlý <sup>1,\*</sup> , Marián Haršáni <sup>2</sup>, Adam Frkáň <sup>2</sup>, Tomáš Fiantok <sup>1</sup>, Martin Sahul <sup>3,4</sup>, Tomáš Roch <sup>5</sup> , Peter Kúš <sup>5</sup> and Marián Mikula <sup>5,6</sup> 

- <sup>1</sup> Detached Workplace of Faculty of Mathematics, Physics and Informatics, Comenius University in Bratislava, Sadová 1148, 038 53 Turany, Slovakia
- <sup>2</sup> STATON, s.r.o., Sadová 1148, 038 53 Turany, Slovakia
- <sup>3</sup> Department of Manufacturing Technology, Faculty of Mechanical Engineering, Czech Technical University in Prague, Technická 4, 166 07 Prague, Czech Republic
- <sup>4</sup> Institute of Materials Science, Faculty of Materials Science and Technology in Trnava, Slovak University of Technology in Bratislava, J. Bottu 25, 917 24 Trnava, Slovakia
- <sup>5</sup> Department of Experimental Physics, Faculty of Mathematics, Physics and Informatics, Comenius University in Bratislava, Mlynská dolina F2, 842 48 Bratislava, Slovakia
- <sup>6</sup> Institute of Materials and Machine Mechanics SAS, Dúbravská cesta 9, 845 11 Bratislava, Slovakia
- \* Correspondence: martin.truchly@fmph.uniba.sk

**Abstract:** Doping of transition metal diborides (TMB<sub>2</sub>) films with soft metals (Ag, Au, Pt) can extend their application potential to tribological and biomedical fields. Here, a combination of direct current unbalanced magnetron sputtering (DC-UBMS) with high-power pulsed magnetron sputtering (HiPIMS) was used to synthesize silver-doped CrB<sub>2+x</sub> thin films on unheated substrates. All Ag–CrB<sub>2+x</sub> thin films were over-stoichiometric with a B/Cr ratio ranging from 2.05 to 2.30 and silver content varying from 3 at.% to 29 at.%. X-ray diffraction demonstrates the amorphous character of the structure in the case of films with silver content ranging from 0 at.% to 8 at.%. A nanocrystalline structure containing a cubic Ag phase is formed in the films with higher silver content. The highest hardness of 26.6 GPa accompanied by the highest value of elastic modulus of 362 GPa was measured in undoped CrB<sub>2.3</sub> films. As the silver content in the Ag–CrB<sub>2+x</sub> thin films increases, the hardness and elastic modulus values gradually decrease to 7.8 GPa and 187 GPa, respectively. The friction properties of CrB<sub>2.3</sub> films, expressed by the coefficient of friction against a steel ball of 0.72, are insufficient and limit their use in demanding industrial applications. However, silver doping significantly reduces the friction coefficient when the lowest value of 0.39 is measured in moderately hard Ag–CrB<sub>2+x</sub> films with an Ag content of 17 at.%. The scratch test shows satisfactory adhesion of films to substrates even without additional heating during deposition.

**Keywords:** chromium diboride; silver; HiPIMS; mechanical properties; tribology



**Citation:** Truchlý, M.; Haršáni, M.; Frkáň, A.; Fiantok, T.; Sahul, M.; Roch, T.; Kúš, P.; Mikula, M. First Approach to Doping Silver into CrB<sub>2</sub> Thin Films Deposited by DC/HiPIMS Technology in Terms of Mechanical and Tribological Properties. *Coatings* **2023**, *13*, 824. <https://doi.org/10.3390/coatings13050824>

Academic Editors: Yuan-Chang Liang and Ajay Vikram Singh

Received: 24 March 2023

Revised: 11 April 2023

Accepted: 21 April 2023

Published: 24 April 2023



**Copyright:** © 2023 by the authors. Licensee MDPI, Basel, Switzerland. This article is an open access article distributed under the terms and conditions of the Creative Commons Attribution (CC BY) license (<https://creativecommons.org/licenses/by/4.0/>).

## 1. Introduction

Transition metal diborides (TMBs) have received a lot of interest in recent decades due to their excellent properties, such as high melting temperature, chemical and thermal stability, high electrical and thermal conductivity, and high hardness level [1–4]. Among them, TiB<sub>2</sub> is probably the most studied [5]. Over-stoichiometric TiB<sub>2+x</sub> thin films with a super-hardness of >40 GPa have a complex self-organized nanostructure that is thermally stable up to 700 °C [4]. Disruptions in the hexagonal microstructure caused by non-stoichiometry prevent dislocations from spreading throughout the unique nanostructure [4,6,7] and explain the high hardness level.

Among the TMBs, chromium diboride (CrB<sub>2</sub>) has received less attention [8–15] but also offers promising properties. In bulk form, it possesses a melting temperature of

2200 °C, a high bulk modulus (211 GPa), oxidation resistance up to 1000 °C, a low thermal expansion coefficient, good wear resistance, and chemical inertness [7]. Compared to TiB<sub>2</sub>, CrB<sub>2</sub> has better corrosion resistance [16]. Thus, CrB<sub>2</sub> is a promising candidate for various high-temperature applications.

Several methods were used for CrB<sub>2</sub> thin-film preparation, including, among others, physical vapor deposition (PVD) methods such as magnetron sputtering. In contrast to related diborides, the CrB<sub>2-x</sub> system has under-stoichiometric tendencies (B/Cr < 2) when prepared by PVD methods [10,17]. Thus, the deposition of close-to-stoichiometric thin films with desired properties is a challenge. Dahm et al. [12] prepared CrB<sub>2</sub> thin films by an unbalanced magnetron sputtering method at temperatures below 200 °C with high hardness in the range of 42–49 GPa. Most of them had a strong (001) orientation, but the exact stoichiometry was not declared. Audronis et al. [8] prepared fully dense and crystalline CrB<sub>2±x</sub> thin films with a strong (001) orientation by pulsed magnetron sputtering. CrB<sub>2</sub> thin films were prepared in a wide concentration range with a B/Cr ratio from 0.92 to 2.3. The largest hardness of 39 GPa was observed for stoichiometric nanocrystalline thin films. Excess boron led to a hardness decrease but the nanocrystalline structure remained. CrB<sub>2.3</sub> thin film had a hardness of 33.2 GPa. On the other hand, boron deficiency led to X-ray amorphous structure and a significant decrease in hardness. A different approach was used by Choi et al. [16], where CrB<sub>2</sub> thin films were deposited by inductively coupled plasma-assisted direct current magnetron sputtering (ICP-DCMS). By changing deposition parameters, the orientation varied between (101) to (001) type and the hardness of thin films was in the range from 30 to 54 GPa. Stoichiometric and hard CrB<sub>2</sub> thin films were also prepared by DC magnetron sputtering [10,15]. Zhang et al. [15] studied the influence of deposition temperature on microstructure and mechanical properties. The deposition temperature changed from 100 °C to 400 °C and the B/Cr ratio varied between 1.94 and 2.06. With increasing temperature, the coating texture changed from a random mixed orientation to the preferred (001) orientation and a super-hardness of 51 GPa was achieved for the highest temperature. Dorri et al. [10] prepared close-to-stoichiometric CrB<sub>2</sub> thin films with a B/Cr ratio from 1.9 to 2.08 and (001) texture at substrate temperatures of 500 °C and 900 °C.

In terms of tribological properties of CrB<sub>2</sub> thin films, pulsed magnetron sputtered films exhibited coefficients of friction (COFs) of ~0.55 [9], ~0.6 [9], and ~0.5 [14] against aluminum alloy, steel, and WC–Co, respectively. Such values are too high for low-friction applications and/or wear-resistant coatings and, thus, improvement of tribological properties is desirable. Doping of thin films with soft metals such as silver could be one of the possibilities.

Several research groups focused on doping silver into nitride films such as TiN [18] or CrN [19–22] to study the tribological, mechanical, and even antimicrobial properties. Soft and ductile silver plastically shears between the sliding surfaces and, therefore, offers a lubricating function [18,23]. An increase in silver content provides a reduction in the coefficient of friction but also a reduction in mechanical hardness and elastic modulus. According to [20,22], decreasing the indentation hardness does not have to be connected to a decrease in wear resistance. On the contrary, wear resistance may be improved.

In this work, we provide the first approach to doping silver into CrB<sub>2+x</sub> thin films deposited by DC/HiPIMS technology. Undoped CrB<sub>2+x</sub> and Ag–CrB<sub>2+x</sub> thin films with different silver contents are analyzed in terms of mechanical and tribological properties. Depending on the stoichiometry, friction properties and specific wear rate are improved at the expense of hardness and elastic modulus. Moreover, Ag–CrB<sub>2+x</sub> thin films exhibit sufficient adhesion on unheated WC–Co substrates.

## 2. Materials and Methods

CrB<sub>2</sub>, Ag, and Ag–CrB<sub>2+x</sub> films were prepared by DC/HiPIMS magnetron co-sputtering in the STATON OCTOMAG coating equipment (STATION, Turany, Slovakia) in the Ar atmosphere on polished WC–Co and Si (001) substrates. Ag (D100 × 6 mm, 99.5% purity,

Kremnica mint, Kremnica, Slovakia) and CrB<sub>2</sub> (D100 × 6 mm, 99.5% purity, Testbourne, Basingstoke, UK) targets were used. Cr target (D100 × 6 mm, 99.95% purity, Testbourne, Basingstoke, UK) was used for the deposition of the 150 nm thick Cr buffer layer. Ag was sputtered by a DC power supply, while CrB<sub>2</sub> was sputtered by a HiPIMS power supply. Prior to depositions, the substrates were ultrasonically cleaned in acetone and isopropyl alcohol and rinsed with distilled water for 5 min.

Before the deposition, the chamber was evacuated to the base pressure of  $5 \times 10^{-3}$  Pa. Substrates were plasma etched using Ar<sup>+</sup> glow discharge working at  $-800$  V for 30 min, and then additionally etched by Ar<sup>+</sup> ions using ion source operating at a voltage of  $-2000$  V and a pressure of 0.1 Pa. A substrate bias was set to  $-800$  V. Prior to each deposition, the targets were pre-sputtered for 5 min at the same Ar pressure and target power as used for the deposition. The frequency and pulse time of the HiPIMS discharge on the CrB<sub>2</sub> target were set to 100 Hz and 250  $\mu$ s, respectively. The CrB<sub>2</sub> discharge was synchronized with the bias power supply. A negative bias of  $-60$  V was applied to the substrate holder during deposition. The peak power for the CrB<sub>2</sub> target was  $\sim 71$ – $78$  kW, and the DC power for the Ag target varied in the range from 30 W to 110 W in order to obtain different silver compositions. For all depositions,  $p_{Ar}$  was  $0.40 \pm 0.02$  Pa corresponding to an Ar flow of 155 sccm. Deposition parameters are summarized in Table 1. The DC/HiPIMS co-depositions of Ag–CrB<sub>2+x</sub> films were performed without substrate heating, and thin films were grown on substrates heated only by ion bombardment during plasma etching and ion irradiation. The deposition time was 50 min; the thickness of the prepared thin films is summarized in Table 2.

**Table 1.** Summary of EDS chemical composition, deposition parameters, and films thickness of CrB<sub>2.3</sub>, Ag–CrB<sub>2+x</sub>, and Ag thin films.

Film Sample	EDS		Deposition Parameters							
	Ratio B/Cr	Ag [at.%]	I <sub>CrB2</sub> [A]	U <sub>CrB2</sub> [V]	P <sub>CrB2</sub> [kW]	f <sub>CrB2</sub> [Hz]	pt <sub>CrB2</sub> [ $\mu$ s]	P <sub>Ag</sub> [W]	I <sub>b</sub> [A]	Thickness [ $\mu$ m]
CrB <sub>2.3</sub>	2.30	0			78			-	1.5	1.1
Ag 3%	2.20	3 ± 1			78			30	1.4	1.2
Ag 8%	2.20	8 ± 1			73			40	1.5	1.3
Ag 13%	2.18	13 ± 1	70	1300	71	100	250	50	1.5	1.3
Ag 17%	2.15	17 ± 1			71			60	1.5	1.4
Ag 18%	2.05	18 ± 1			77			70	1.6	1.5
Ag 29%	2.30	29 ± 1			77			110	1.6	1.9
Ag	-	100	-	-	-	-	-	110	0.1	1.4

**Table 2.** Summary of hardness H, elastic modulus E, coefficient of friction COF, and specific wear rate of CrB<sub>2.3</sub>, Ag–CrB<sub>2+x</sub>, and Ag thin films.

	H [GPa]	E [GPa]	COF	Specific Wear Rate [m <sup>3</sup> /Nm]
CrB <sub>2.3</sub>	26.6 ± 1.1	362 ± 11	0.72	1.61 × 10 <sup>-13</sup>
Ag 3%	22.1 ± 0.8	325 ± 8	0.71	9.51 × 10 <sup>-14</sup>
Ag 8%	18.3 ± 1.2	299 ± 9	0.49	8.38 × 10 <sup>-14</sup>
Ag 13%	15.0 ± 0.6	268 ± 12	0.48	1.09 × 10 <sup>-13</sup>
Ag 17%	13.1 ± 0.2	245 ± 5	0.29	1.12 × 10 <sup>-13</sup>
Ag 18%	11.4 ± 0.1	231 ± 5	0.32	1.27 × 10 <sup>-13</sup>
Ag 29%	7.8 ± 0.1	187 ± 4	0.36	1.39 × 10 <sup>-13</sup>
Ag	1.2 ± 0.5	97 ± 27	0.39	6.10 × 10 <sup>-15</sup>

The chemical composition of the thin films was measured using energy-dispersive X-ray spectroscopy (INCA Oxford Instruments, Oxford, England) attached to the TESCAN VEGA scanning electron microscope (SEM, TESCAN, Brno, Czech Republic). The accelerating voltage was set to 10 keV. Before EDS measurements, calibration standards of the pure elements Cr, B, and Ag were used.

The structural analysis was carried out by X-ray diffraction (XRD) using PANalytical X'pert Pro MRD diffractometer (PANalytical, Almelo, The Netherlands) equipped with  $\text{CuK}\alpha$  ( $\lambda = 0.15418$  nm) radiation source and operating in standard Bragg–Brentano geometry.

Mechanical properties, including hardness and elastic modulus, were measured by the nanoindentation method using nanoindenter Anton Paar NHT<sup>2</sup> (Anton Paar, Graz, Austria) equipped with a standard diamond Berkovich tip and determined via the Oliver and Pharr method [24]. The penetration depth was less than 10% of the overall thickness to minimize the influence of the substrate. Twenty valid indents ( $5 \times 4$  matrix) were performed on each sample.

Adhesion properties were evaluated by a scratch test. The Bruker UMT-2 device (Bruker, Billerica, MA, USA) was used to determine the adhesion properties in terms of progressive loading up to 60 N. The evaluation of scratches was performed using SEM, and critical load values  $L_c$  were determined according to [25].

For tribological properties, the Bruker UMT-2 device in ball-on-disc setup was used to determine the coefficient of friction as a function of silver content in the Ag–CrB<sub>2+x</sub> thin films. Parameters for ball-on-disc were as follows: load force of 2 N, rotation of 200 rpm, race-track radius of 2.5 mm, time of 12 min, a sliding distance of 31.5 m, and a counterpart of 100Cr6 bearing steel ball with a diameter of 6.3 mm. During the test, temperature and relative humidity were 23.5 °C and 30%–33%, respectively. It should be emphasized that the given temperature is the ambient temperature and the sample is not intentionally heated during the measurement. However, the real temperature is higher because of the frictional heat produced at the tribo-contact. The volume of worn material from wear tracks after the ball-on-disc test was measured by confocal laser microscope Keyence VK-X 1050 (Keyence, Osaka, Japan). Furthermore, all wear tracks were analyzed by SEM in terms of EDS chemical maps and higher magnification.

### 3. Results

#### 3.1. Chemical Composition of Studied Thin Films

Semi-quantitative elemental EDS analysis of the reference sputtered CrB<sub>2+x</sub> films reveals a slightly over-stoichiometric ratio of B/Cr  $\approx$  2.30. According to the elemental analysis of Ag–CrB<sub>2+x</sub> thin films, co-deposition leads to the addition of silver to the growing films in the range from 3 at.% to 29 at.%, while the B/Cr ratio ranges from 2.05 to 2.30. Carbon and oxygen contamination does not exceed a total of 3 at.%. EDS chemical composition of Ag–CrB<sub>2+x</sub> thin films is summarized in Table 1.

#### 3.2. XRD Structure of Ag–CrB<sub>2+x</sub> Thin Films

The evolution of the structure of Ag–CrB<sub>2+x</sub> thin films with various compositions is shown in Figure 1 by the XRD patterns on the selected  $2\theta$  range between 25° and 66°. The absence of CrB<sub>2</sub> reflections in CrB<sub>2.3</sub> thin film suggests an amorphous character of the film. The lower content of silver (up to 8 at.%) in the films does not change the amorphous structure. The XRD patterns of the Ag–CrB<sub>2+x</sub> thin films with higher content of silver (>8 at.%) exhibit increased intensity (compared to the background) and comparatively wider reflections (in range of  $\pm 2.5^\circ$ ) centered at  $2\theta \approx 38^\circ$  and  $44^\circ$ , indicating the presence of a nanocrystalline structure. In the case of the films with the highest content of silver (29 at.%), the narrow XRD reflections (111) and (200) located at  $2\theta \approx 38^\circ$  and  $2\theta \approx 44^\circ$ , respectively, are identified as a cubic silver phase.

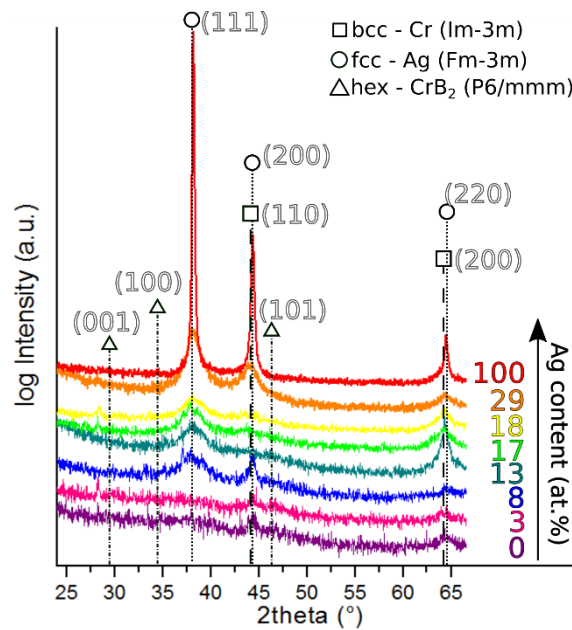


**Figure 1.** X-ray diffraction patterns of Ag–CrB<sub>2+x</sub> thin films as a function of Ag content.

### 3.3. Cross-Section of Ag–CrB<sub>2+x</sub> Thin Films

Figure 2 depicts SEM cross-section micrographs of studied thin films. The cross-section structure exhibits dense (nonporous) morphology in all cases and a glassy structure with the Ag content up to 18 at.%, which is in good agreement with the amorphous structure measured by XRD.

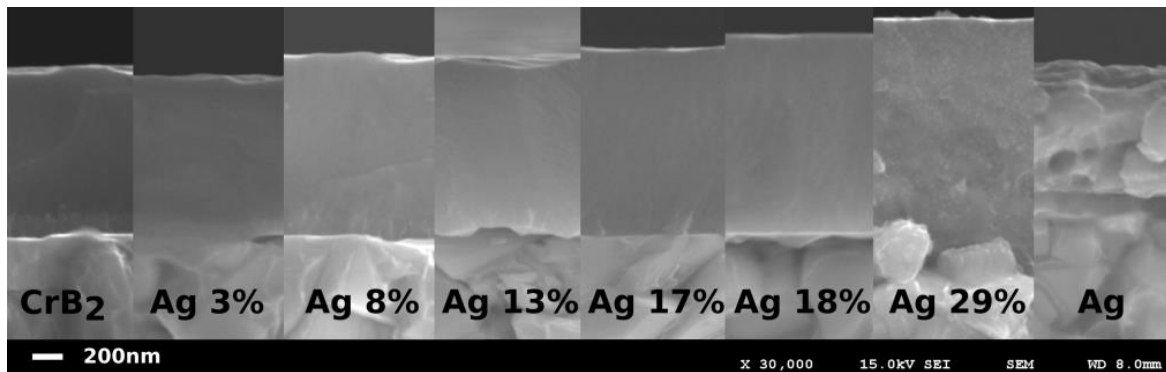


**Figure 2.** SEM micrographs of cross-section of Ag–CrB<sub>2+x</sub> thin films as a function of the silver content.

In the case of Ag 29%, the glassy and smooth structure disappears, and changes to a globular-like morphology. Since the XRD reveals the crystalline nature of silver in all samples, we assume that silver distributed in the film tends to aggregate and form larger grains at a higher Ag content, which are embedded in an amorphous a-CrB<sub>x</sub> phase.

### 3.4. Mechanical Properties of Ag–CrB<sub>2+x</sub> Thin Films

The effect of structural evolution on the mechanical properties of Ag–CrB<sub>2+x</sub> films as a function of the silver content is presented in Figure 3. The reference CrB<sub>2.3</sub> film has a hardness  $H$  of  $26.6 \pm 1.1$  GPa and an elastic modulus  $E$  of  $362 \pm 11$  GPa, which is comparable to the previously published hardness values of X-ray amorphous CrB<sub>2</sub> films [9]. However, doping with silver causes a monotonous decrease in hardness and elastic moduli. For the sample with the Ag content of 29 at.%, hardness and elastic modulus decrease to  $7.8 \pm 0.1$  GPa and  $187 \pm 4$  GPa, respectively.

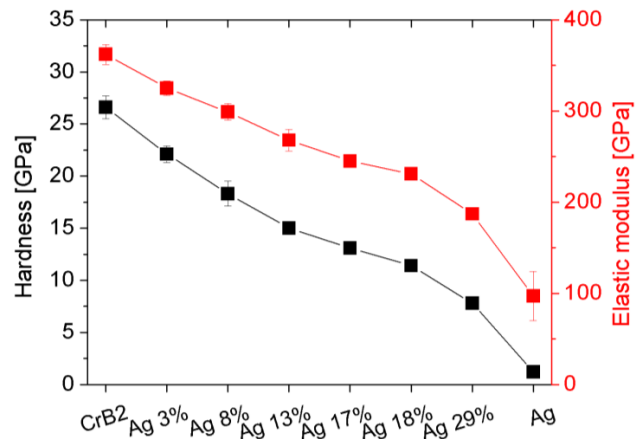


**Figure 3.** Hardness and elastic modulus of Cr, Ag, and Ag–CrB<sub>2+x</sub> thin films.

We assume that such a significant change in mechanical properties is caused by the fact that silver is an insoluble element in CrB<sub>2</sub> and does not form hard nitrides or borides, but rather precipitates at grain boundaries and forms a soft metal matrix [26]. In such a case, the lower hardness may be attributed to a dislocation-based homogeneous plastic deformation mechanism in the soft metal matrix due to the low shear strength of silver. The reference sample of silver deposited by DC magnetron sputtering shows a hardness and elastic modulus of  $1.2 \pm 0.5$  GPa and  $97 \pm 27$  GPa, respectively.

### 3.5. Adhesion Properties of Ag–CrB<sub>2+x</sub> Thin Films

As measured by the scratch test, CrB<sub>2+x</sub> and Ag–CrB<sub>2+x</sub> thin films have sufficient adhesion on WC–Co substrates despite the low deposition temperatures. For all samples, the critical load is over 35 N and adhesive failure in the form of wedging spallation occurs in some cases at higher loads. The reference Ag thin film exhibits good adhesive strength with a critical load over 60 N and no internal cracks or delamination from the substrate. Overall, the films' adhesion on the WC–Co substrates is slightly improved by adding silver to the CrB<sub>2+x</sub> thin films.

### 3.6. Tribological Response of Silver-Doped CrB<sub>2+x</sub> Thin Films

The coefficient of friction of the Ag–CrB<sub>2+x</sub> thin films against 100Cr6 steel was measured by the ball-on-disc test (Figure 4A). COFs of reference undoped CrB<sub>2.3</sub> and Ag thin films are 0.72 and 0.39, respectively. The lowest value of COF is observed in the case of Ag 17 at.%, with a value of 0.29. Further incorporation of silver in the Ag–CrB<sub>2+x</sub> thin films gradually leads to an increase in the average value of the coefficient of friction to 0.36 for Ag 29 at.%. In general, the addition of silver into the CrB<sub>2+x</sub> thin films results in a decrease in COF.

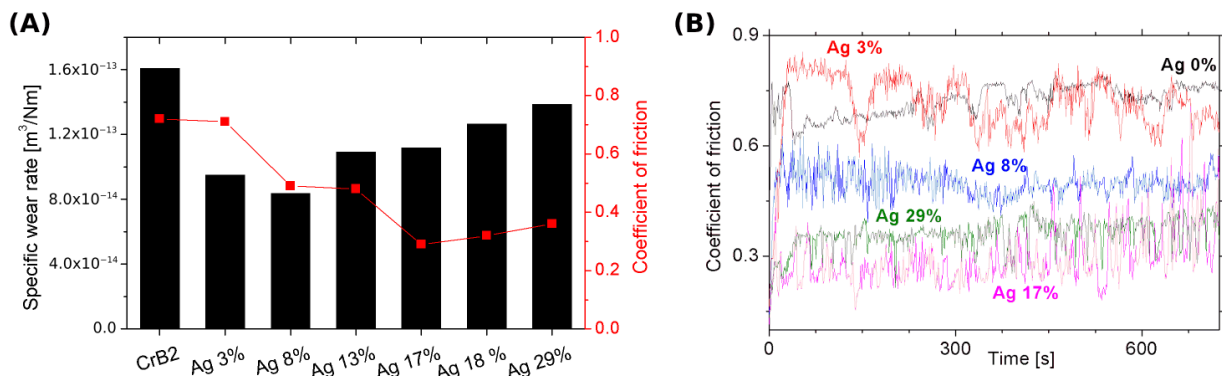


**Figure 4.** (A) Specific wear rate and coefficients of friction of Ag–CrB<sub>2+x</sub> thin films; (B) selected coefficients of friction of Ag–CrB<sub>2+x</sub> thin films during the ball-on-disc test.

Figure 4 depicts the effect of silver on the specific wear rate of the Ag–CrB<sub>2+x</sub> thin films. Although the COF decreases with Ag content up to 17 at.% with a slight increase for higher Ag content, the specific wear rate exhibits a significant non-linear behavior with a valley for the sample Ag 8 at.%, where a value of  $8.38 \times 10^{-14} \text{ m}^3/\text{Nm}$  is measured. This sample maintains a moderate hardness of 18.3 GPa. Two opposite effects take place: the reduction in COF and the loss of hardness of the thin films with increasing Ag content. Additional silver incorporation into the CrB<sub>2+x</sub> results in an increase in the specific wear rate. The thin film with the highest amount of Ag 29 at.% shows the lowest hardness of 7.8 GPa and a specific wear rate of  $1.39 \times 10^{-13} \text{ m}^3/\text{Nm}$ . Although the COF is still reduced, the specific wear rate increases due to the formation of large Ag clusters and the weakening of the CrB<sub>2</sub> matrix.

In general, mechanical hardness and specific wear rate are correlated. It is reasonable to expect that as hardness decreases, so will wear resistance, and vice versa. This statement is partially true if we are talking about mono-structural hard coatings. However, in our experiments supported by other authors [10,17,21,22], there is a nanocomposite CrB<sub>2+x</sub> with a boron tissue phase, and Ag atoms form clusters in the CrB<sub>2+x</sub> matrix. These Ag particles are probably released and reduce friction during sliding. Such a structure, including a crystalline and an amorphous component, can reduce friction and wear despite the lower hardness. In order to achieve the potential of such a structure, it is necessary to ensure a sufficient amount of this lubricating component (in our case, silver), which ensures the formation of a continuous metallic lubrication film.

Mulligan et al. made a similar observation [27] in CrN–Ag thin films, where sufficient silver content in thin films forms a solid lubricating film during the sliding. The more silver used, the faster a lubricating film with greater thickness is formed. In our case, we do not observe a continuous lubricating film. Silver particles are observed in thin film with the Ag 13 at.% and more.

A low COF does not guarantee a low specific wear rate, since the interplay between COF, hardness, and wear is crucial. As shown in Figure 4, the lowest COF among the Ag–CrB<sub>2+x</sub> thin films is for the sample with Ag 17 at.%, but the lowest specific wear rate is observed on the sample with Ag 8 at.%. A higher amount of silver positively influences friction, but the decrease in hardness results in more severe wear. In the case of the samples with an amount of Ag  $\geq 13$  at.%, the latter effect prevails. Good wear resistance is related to the beneficial and reasonable combination of hardness and chemical composition.

In the case of Ag reference thin film, the lowest specific wear rate is influenced by the adhesion of silver from the film to the steel ball. Effectively, there is a silver-to-silver tribo-contact and the average COF value of the Ag thin film is 0.39.

In Figure 5, the SEM–EDS map of the selected sample with Ag 29 at.% depicts the detail of the bottom of the wear track with partially delaminated film from the adhesive Cr layer. As can be further seen in the delaminated region, the strong signal of Cr (cyan) is from the chromium adhesion layer, as is the strong signal of tungsten from the WC/Co substrate. From SEM micrographs and the EDS chemical map of the bottom of the wear track, it is obvious that during the sliding, silver is uniformly distributed over the whole analyzed area, except for the area with delaminated films. In the delaminated area (highlighted by the white arrow) and in the central asperity (highlighted by the red arrows), we observe a higher presence of oxygen.

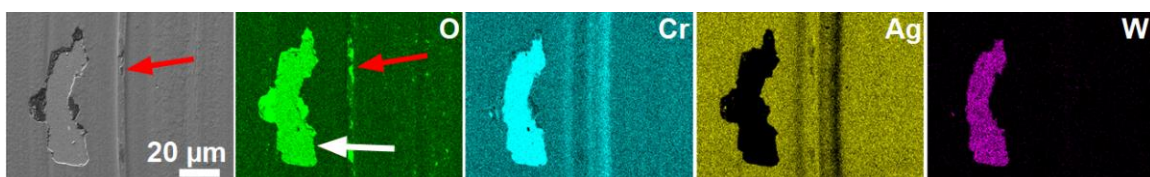


**Figure 5.** EDS chemical map of sample with the Ag 28.8 at.%. Distribution of elements at the bottom of the wear track after ball-on-disc.

During sliding, the material of the steel counterpart is transferred into the film's surface and mixed with a material of  $\text{Ag-CrB}_{2+x}$ . If we consider the lower adhesive strength of thin films, such delaminated film material is then milled inside the wear track, and wear debris is formed. Debris includes the material of the steel ball and particles from the thin film. Under the load of the sliding ball, there is notable intermixing and oxidation of transferred wear debris material. This forms a metal oxide containing transfer film on the film's surface. This loose material acts as an additional abrasive media and facilitates abrasive wear, which is the main wear mechanism. Similar behavior was observed in [9,13].

Abrasive wear and plowed grooves are clearly visible on the surface topography image made by laser confocal microscopy (Figure 6). The abrasive nature of loose  $\text{CrB}_2$  and oxidized debris particles naturally enhance the abrasive wear of the thin films. Oxidized debris/particles are also observed at the bottom of the wear tracks. It was reported in several research papers that during the sliding, a higher temperature (or flash temperature) is generated and supports the oxidation of borides [13,28] and nitrides [29–32]. In our case, the formation of oxides is reduced due to the low applied load of 2 N and the presence of silver, as can be seen on the EDS map of oxygen (Figure 5). This could be explained by the fact that soft metals have excellent heat conductivity, since they can diffuse out the frictional heat generated at the contact. A similar observation was made by Erdemir [33]. According to Kalin [34], measuring the exact flash temperature is difficult due to the different temperature models that could be used and the experimental setup.

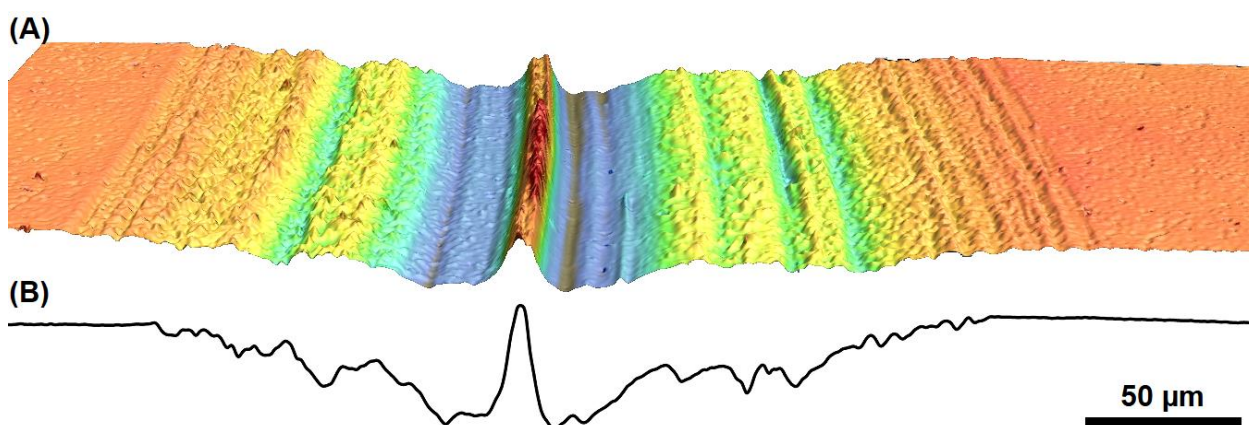


**Figure 6.** (A) Wear track topography of sample with Ag content of 29 at.%. The 3D profile measured by laser confocal microscope with grooves after abrasive sliding of a steel ball. (B) The 2D profile of the same wear track.

In Figure 7, SEM micrographs depict wear-related defects of worn  $\text{Ag-CrB}_{2+x}$  thin films. Here, the  $\text{CrB}_{2.3}$  thin film with strong delamination from the substrate is observed (highlighted by the green arrow). As discussed above, lower coating-to-substrate adhesion accelerates the wear rate of thin films due to the faster formation of wear debris. Cracks formed in the tribo-oxide layer are perpendicular to the sliding direction due to tensile stresses caused by the sliding ball and the applied load. The SEM micrograph in Figure 7B of Ag 3 at.% depicts a notable improvement in the wear rate (see also Figure 4A) and its nature. Adhesive delamination of the thin film from the substrate (highlighted by the green arrow) is lower than for  $\text{CrB}_{2.3}$ . In the case of Ag 17 at.% thin film, increased silver content results in the lowest COF, attributed to the formation of the metal lubricating film. During the sliding and plowing of the steel ball, silver grains/particles are abrasively exposed and released from the thin film, and their spreading over the surface of the wear track can be seen.

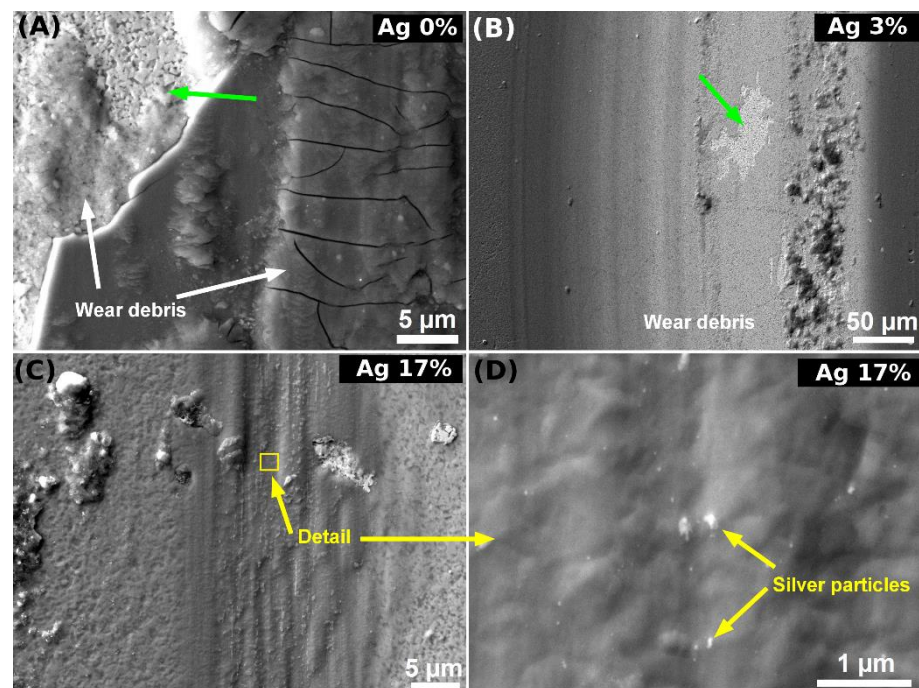


**Figure 7.** (A) SEM micrographs of worn Ag–CrB<sub>2+x</sub> thin films. CrB<sub>2.3</sub> with Ag 0 at.% with delaminated film from the substrate and tribo-oxidation of the films at the bottom of the wear track. (B) Minor delamination of the thin film from the substrate in the case of Ag 3 at.%. (C) Ag 17 at.% with silver particles (aggregates) on the film’s surface after the ball-on-disc. (D) A closer look at the silver particles.

#### 4. Conclusions

To conclude, a combination of direct current unbalanced magnetron sputtering and high-power pulsed magnetron sputtering (HiPIMS) was used to synthesize silver-doped Ag–CrB<sub>2+x</sub> thin films on unheated substrates. Over-stoichiometric Ag–CrB<sub>2+x</sub> films contain silver in the range from 3 to 29 at.%. While thin films with lower Ag content are X-ray amorphous in terms of structure, films with higher Ag content have a nanocomposite structure containing silver grains embedded in an amorphous a-CrB<sub>x</sub> matrix.

The CrB<sub>2.3</sub> thin film exhibits the highest hardness of 26.6 GPa and elastic modulus of 362 GPa. The addition of silver leads to a decrease in the hardness of Ag–CrB<sub>2+x</sub> from 22.1 GPa to 7.8 GPa, accompanied by a monotonic decrease in elastic modulus from 325 GPa to 187 GPa. Ag–CrB<sub>2+x</sub> films exhibit sufficient adhesion and the critical load is over 35 N. Doping CrB<sub>2+x</sub> with silver significantly improves the frictional properties when the coefficient of friction decreases from 0.71 to 0.29. In addition, an improvement in the wear rate of the films is observed due to the formation of a lubricating metal film. The studied silver-doped over-stoichiometric CrB<sub>2+x</sub> film appears to be a promising candidate for tribological applications where moderate hardness combined with low COF is required. In addition, this ceramic composite containing silver particles can also find application in the biomedical field.

**Author Contributions:** Conceptualization, M.T. and M.H.; methodology, M.H.; validation, M.T., M.H. and T.F.; formal analysis, M.H.; investigation, M.T., M.H., M.S. and T.R.; resources, A.F.; data curation, M.T. and M.H.; writing—original draft preparation, M.T. and M.H.; writing—review and editing, M.M., T.R. and T.F.; visualization, M.H. and M.T.; supervision, M.M.; project administration, P.K. and M.M. All authors have read and agreed to the published version of the manuscript.

**Funding:** This work was supported by an Operational Program Integrated Infrastructure (Project No. ITMS 313011AUH4).

**Institutional Review Board Statement:** Not applicable.

**Informed Consent Statement:** Not applicable.

**Data Availability Statement:** The data presented in this study are available from the corresponding author upon request.

**Conflicts of Interest:** The authors declare no conflict of interest.

## References

1. Goncharov, A.A.; Dub, S.N.; Agulov, A.V.; Petukhov, V.V. Structure, Composition, and Mechanical Properties of Thin Films of Transition Metals Diborides. *J. Superhard Mater.* **2015**, *37*, 422–428. [CrossRef]
2. Mitterer, C. Borides in Thin Film Technology. *J. Solid State Chem.* **1997**, *133*, 279–291. [CrossRef]
3. Thörnberg, J.; Palisaitis, J.; Hellgren, N.; Klimashin, F.F.; Ghafoor, N.; Zhirkov, I.; Azina, C.; Battaglia, J.-L.; Kusiak, A.; Sortica, M.A.; et al. Microstructure and Materials Properties of Understoichiometric TiB<sub>x</sub> Thin Films Grown by HiPIMS. *Surf. Coat. Technol.* **2020**, *404*, 126537. [CrossRef]
4. Mayrhofer, P.H.; Mitterer, C.; Wen, J.G.; Greene, J.E.; Petrov, I. Self-Organized Nanocolumnar Structure in Superhard TiB<sub>2</sub> Thin Films. *Appl. Phys. Lett.* **2005**, *86*, 131909. [CrossRef]
5. Munro, R.G. Material Properties of Titanium Diboride. *J. Res. Natl. Inst. Stand. Technol.* **2000**, *105*, 709–720. [CrossRef]
6. Palisaitis, J.; Dahlqvist, M.; Hall, A.J.; Thörnberg, J.; Persson, I.; Nedfors, N.; Hultman, L.; Greene, J.E.; Petrov, I.; Rosen, J.; et al. Where Is the Unpaired Transition Metal in Substoichiometric Diboride Line Compounds? *Acta Mater.* **2021**, *204*, 116510. [CrossRef]
7. Emiliani, M.L. Characterization and Oxidation Resistance of Hot-Pressed Chromium Diboride. *Mater. Sci. Eng. A* **1993**, *172*, 111–124. [CrossRef]
8. Audronis, M.; Kelly, P.J.; Arnell, R.D.; Valiulis, A.V. Pulsed Magnetron Sputtering of Chromium Boride Films from Loose Powder Targets. *Surf. Coat. Technol.* **2006**, *200*, 4166–4173. [CrossRef]
9. Audronis, M.; Rosli, Z.M.; Leyland, A.; Kelly, P.J.; Matthews, A. Tribological Behaviour of Pulsed Magnetron Sputtered CrB<sub>2</sub> Coatings Examined by Reciprocating Sliding Wear Testing against Aluminium Alloy and Steel. *Surf. Coat. Technol.* **2008**, *202*, 1470–1478. [CrossRef]
10. Dorri, M.M.; Thörnberg, J.; Hellgren, N.; Palisaitis, J.; Petruhins, A.; Klimashin, F.F.; Hultman, L.; Petrov, I.; Persson, P.O.Å.; Rosen, J. Synthesis and Characterization of CrB<sub>2</sub> Thin Films Grown by DC Magnetron Sputtering. *Scr. Mater.* **2021**, *200*, 113915. [CrossRef]
11. Marka, S.; Menaka; Ganguli, A.K.; Krishna, M.G. Effect of Substrate and Film Thickness on the Growth, Structure, Mechanical and Optical Properties of Chromium Diboride Thin Films. *Surf. Coat. Technol.* **2012**, *209*, 23–31. [CrossRef]
12. Dahm, K.L.; Jordan, L.R.; Haase, J.; Dearnley, P.A. Magnetron Sputter Deposition of Chromium Diboride Coatings. *Surf. Coat. Technol.* **1998**, *108–109*, 413–418. [CrossRef]
13. Bhatt, B.; Murthy, T.S.R.C.; Limaye, P.K.; Nagaraj, A.; Singh, K.; Sonber, J.K.; Sairam, K.; Sashanka, A.; Rao, G.V.S.N.; Rao, T.S. Tribological Studies of Monolithic Chromium Diboride against Cemented Tungsten Carbide (WC–Co) under Dry Condition. *Ceram. Int.* **2016**, *42*, 15536–15546. [CrossRef]
14. Cheng, C.-H.; Lee, J.-W.; Ho, L.-W.; Chen, H.-W.; Chan, Y.-C.; Duh, J.-G. Microstructure and Mechanical Property Evaluation of Pulsed DC Magnetron Sputtered Cr–B and Cr–B–N Films. *Surf. Coat. Technol.* **2011**, *206*, 1711–1719. [CrossRef]
15. Zhang, S.; Wang, Z.; Guo, P.; Ke, P.; Odén, M.; Wang, A. Temperature Induced Superhard CrB<sub>2</sub> Coatings with Preferred (001) Orientation Deposited by DC Magnetron Sputtering Technique. *Surf. Coat. Technol.* **2017**, *322*, 134–140. [CrossRef]
16. Choi, H.S.; Park, B.; Lee, J.J. CrB<sub>2</sub> Coatings Deposited by Inductively Coupled Plasma Assisted DC Magnetron Sputtering. *Surf. Coat. Technol.* **2007**, *202*, 982–986. [CrossRef]
17. Nedfors, N.; Primetzhofer, D.; Wang, L.; Lu, J.; Hultman, L.; Jansson, U. Characterization of magnetron sputtered Cr–B and Cr–B–C thin films for electrical contact applications. *Surf. Coat. Technol.* **2015**, *266*, 167–176. [CrossRef]
18. Sliney, H.E. The Use of Silver in Self-Lubricating Coatings for Extreme Temperatures. *ASLE Trans.* **1986**, *29*, 370–376. [CrossRef]
19. Bilek, P.; Jurci, P.; Novak, M.; Hudakova, M.; Caplovic, L. Tribological and Mechanical Properties of Cr<sub>2</sub>N–11Ag-Coatings Deposited on Cr–V Ledeburitic Steel. *Wear* **2015**, *340–341*, 47–52. [CrossRef]
20. Kelly, P.J.; Li, H.; Benson, P.S.; Whitehead, K.A.; Verran, J.; Arnell, R.D.; Iordanova, I. Comparison of the Tribological and Antimicrobial Properties of CrN/Ag, ZrN/Ag, TiN/Ag, and TiN/Cu Nanocomposite Coatings. *Surf. Coat. Technol.* **2010**, *205*, 1606–1610. [CrossRef]
21. Mulligan, C.P.; Blanchet, T.A.; Gall, D. CrN–Ag Nanocomposite Coatings: Effect of Growth Temperature on the Microstructure. *Surf. Coat. Technol.* **2008**, *203*, 584–587. [CrossRef]
22. Mulligan, C.P.; Blanchet, T.A.; Gall, D. CrN–Ag Nanocomposite Coatings: High-Temperature Tribological Response. *Wear* **2010**, *269*, 125–131. [CrossRef]
23. 9 Solid Lubrication and Surface Treatments. In *Tribology Series; Engineering Tribology*; Stachowiak, G.W.; Batchelor, A.W. (Eds.) Elsevier: Amsterdam, The Netherlands, 1993; Volume 24, pp. 485–526.
24. Oliver, W.C.; Pharr, G.M. An improved technique for determining hardness and elastic modulus using load and displacement sensing indentation experiments. *J. Mater. Res.* **1992**, *7*, 1564–1583. [CrossRef]
25. Standard Test Method for Adhesion Strength and Mechanical Failure Modes of Ceramic Coatings by Quantitative Single Point Scratch Testing. Available online: <https://www.astm.org/c1624-05.html> (accessed on 1 February 2023).

26. Musil, J.; Zeman, P.; Baroch, P. Hard Nanocomposite Coatings. In *Comprehensive Materials Processing*; Elsevier: Amsterdam, The Netherlands, 2014; pp. 325–353. ISBN 978-0-08-096533-8.
27. Mulligan, C.P.; Blanchet, T.A.; Gall, D. CrN–Ag Nanocomposite Coatings: Tribology at Room Temperature and during a Temperature Ramp. *Surf. Coat. Technol.* **2010**, *204*, 1388–1394. [[CrossRef](#)]
28. Sonber, J.K.; Raju, K.; Murthy, T.S.R.C.; Sairam, K.; Nagaraj, A.; Majumdar, S.; Kain, V. Friction and Wear Properties of Zirconium Diboride in Sliding against WC Ball. *Int. J. Refract. Met. Hard Mater.* **2018**, *76*, 41–48. [[CrossRef](#)]
29. Ashby, M.F.; Abulawi, J.; Kong, H.S. Temperature Maps for Frictional Heating in Dry Sliding. *Tribol. Trans.* **1991**, *34*, 577–587. [[CrossRef](#)]
30. Yalamanchili, K.; Jiménez-Piqué, E.; Pelcastre, L.; Bakoglidis, K.D.; Roa, J.J.; Johansson Jöesaar, M.P.; Prakash, B.; Ghafoor, N.; Odén, M. Influence of Microstructure and Mechanical Properties on the Tribological Behavior of Reactive Arc Deposited Zr-Si-N Coatings at Room and High Temperature. *Surf. Coat. Technol.* **2016**, *304*, 393–400. [[CrossRef](#)]
31. Polcar, T.; Martinez, R.; Vítů, T.; Kopecký, L.; Rodriguez, R.; Cavaleiro, A. High Temperature Tribology of CrN and Multilayered Cr/CrN Coatings. *Surf. Coat. Technol.* **2009**, *203*, 3254–3259. [[CrossRef](#)]
32. Wu, F.; Yu, L.; Ju, H.; Asempah, I.; Xu, J. Structural, Mechanical and Tribological Properties of NbCN-Ag Nanocomposite Films Deposited by Reactive Magnetron Sputtering. *Coatings* **2018**, *8*, 50. [[CrossRef](#)]
33. Erdemir, A.; Busch, D.E.; Erck, R.A.; Fenske, G.R.; Lee, R. *Ion-Beam-Assisted Deposition of Silver Films on Zirconia Ceramics for Improved Tribological Behavior*; Argonne National Lab. (ANL): Argonne, IL, USA, 1990.
34. Kalin, M. Influence of Flash Temperatures on the Tribological Behaviour in Low-Speed Sliding: A Review. *Mater. Sci. Eng. A* **2004**, *374*, 390–397. [[CrossRef](#)]

**Disclaimer/Publisher’s Note:** The statements, opinions and data contained in all publications are solely those of the individual author(s) and contributor(s) and not of MDPI and/or the editor(s). MDPI and/or the editor(s) disclaim responsibility for any injury to people or property resulting from any ideas, methods, instructions or products referred to in the content.